# Rheological and Tribological Properties of Carbon Nanotube/Thermoplastic Nanocomposites Incorporating Inorganic Fullerene-Like WS$_2$ Nanoparticles

Ana M. Díez-Pascual,*[,†] Mohammed Naffakh,[†,‡] Carlos Marco,[†] and Gary Ellis[†]

[†]Instituto de Ciencia y Tecnología de Polímeros, ICTP-CSIC, Juan de la Cierva 3, 28006 Madrid, Spain
[‡]Departamento de Ingeniería y Ciencia de Los Materiales, Escuela Técnica Superior de Ingenieros Industriales, Universidad Politécnica de Madrid, José Gutiérrez Abascal 2, 28006 Madrid, Spain

ABSTRACT: The rheological and tribological properties of single-walled carbon nanotube (SWCNT)-reinforced poly(phenylene sulphide) (PPS) and poly(ether ether ketone) (PEEK) nanocomposites prepared via melt-extrusion were investigated. The effectiveness of employing a dual-nanofiller strategy combining polyetherimide (PEI)-wrapped SWCNTs with inorganic fullerene-like tungsten disulfide (IF-WS$_2$) nanoparticles for property enhancement of the resulting hybrid composites was evaluated. Viscoelastic measurements revealed that the complex viscosity η, storage modulus G′, and loss modulus G″ increased with SWCNT content. In the low-frequency region, G′ and G″ became almost independent of frequency at higher SWCNT loadings, suggesting a transition from liquid-like to solid-like behavior. The incorporation of increasing IF-WS$_2$ contents led to a progressive drop in η and G′ due to a lubricant effect. PEEK nanocomposites showed lower percolation threshold than those based on PPS, ascribed to an improved SWCNT dispersion due to the higher affinity between PEI and PEEK. The SWCNTs significantly lowered the wear rate but only slightly reduced the coefficient of friction. Composites with both nanofillers exhibited improved wear behavior, attributed to the outstanding tribological properties of these nanoparticles and a synergistic reinforcement effect. The combination of SWCNTs with IF-WS$_2$ is a promising route for improving the tribological and rheological performance of thermoplastic nanocomposites.
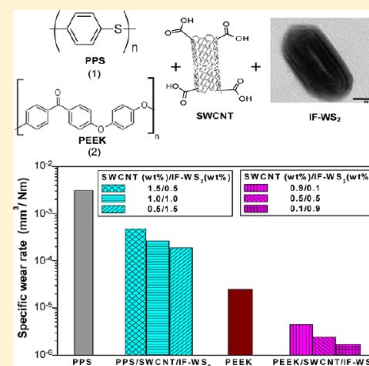
1. INTRODUCTION

Composites incorporating carbon nanotubes (CNTs) within a polymeric matrix have attracted considerable attention in both research and industry due to their good electrical and thermal conductivity, high stiffness and strength at relatively low CNT content.[1] However, a major challenge in the development of such composite materials is to obtain a homogeneous dispersion of the nanofillers within the polymer matrix that remains to be a very difficult task due to the strong intermolecular van der Waals interactions between CNTs and their large surface area, which result in the formation of aggregates. Another factor that limits the improvement in properties is the CNT-polymer interfacial interaction, since a strong adhesion is required in order to attain effective load transfer between the composite phases. Currently, solution mixing,[2] melt compounding,[3] and in situ polymerization[4] are commonly used to prepare this type of nanocomposites. From a materials production viewpoint, the melt-blending approach can be more convenient than the others since it is compatible with conventional industrial processes, such as extrusion, injection and blow molding, thus being easily implemented, and has the advantage that aggregate formation can be reduced by the application of shear during mixing.

For the processing and application of CNT-reinforced polymer nanocomposites, the rheological and tribological properties are of great importance. These properties are influenced by the morphology of the material in terms of degree of crystallinity, crystallite size, state of nanofiller dispersion and orientation as well as by the interactions between the CNT network and the entangled polymer chains.[5] Melt rheology is a very sensitive method to characterize nanocomposite melts, and is valuable both for improving processing conditions and for understanding the fundamental characteristics of the materials at the nanoscale. For example, significant changes in the rheological behavior with increasing CNT content at temperatures above the glass transition have been related to percolation effects,[6,7] and changes in the frequency dependence of dynamic moduli and viscosity have been interpreted in the frame of liquid-to-solid or liquid-to-gel transitions, as reported for multiwalled carbon nanotube (MWCNT) reinforced polycarbonate[8] and polyamide-6[9] nanocomposites.

On the other hand, a complete thorough study of the tribological performance is a crucial step to further exploit the potential of high-performance composites for industrial applications. In this respect, significant efforts have been aimed at using various types of fillers. Thus, different strategies have been reported, namely the incorporation of solid

lubricants such as graphite or polytetrafluoroethylene (PTFE) to reduce the coefficient of friction (μ),[10] the addition of fiber reinforcements such as carbon or glass fibers to increase stiffness and strength,[11] as well as the incorporation of hard nanoscale particles to increase mechanical properties and decrease μ.[12] A more recent innovation is the dispersion of inorganic fullerene-like (IF) nanoparticles[13] such as tungsten disulfide, IF-WS$_2$, that possess exceptional properties like high modulus and low μ, attributed to their small size, closed structure, and chemical inertness, making them ideal candidates for improving the mechanical and tribological properties of polymers.[14,15]

Poly(phenylene sulphide) (PPS) and poly(ether ether ketone) (PEEK) are semicrystalline high-performance thermoplastics with high glass transition and melting temperatures, outstanding mechanical and thermal properties, excellent chemical and abrasion resistance, as well as dimensional stability, minimum water absorption, inherent nonflammability, antiaging, and good tribological properties. These polymers are used for a wide range of applications including the electronics, telecommunications, automobile, and aeronautic industries. To extend their structural applications, different fillers such as glass fibers,[16] carbon nanofibers (CNFs),[17] nanoparticles,[12,18,19] CNTs,[3,6,7] as well as nanoparticle/CNT mixtures[20−23] have been melt-blended with these matrices. Most of these studies focused on the thermal and mechanical characterization of the resulting composites, and only limited information on their rheology or wear performance is available. Indeed, to the best of our knowledge, no previous study dealing with the rheological and tribological behavior of SWCNT or IF-nanoparticle reinforced PPS or PEEK composites has been reported to date.

The main goal of this work is to analyze the influence of SWCNT dispersion and loading on the rheological and tribological properties of PPS and PEEK matrices and correlate the results with the morphology of the materials. To improve the distribution of the nanotubes and tailor the polymer/SWCNT interface while preserving the integrity of the tubes, polyetherimide (PEI) was used as a compatibilizing agent. Furthermore, the effect of replacing part of the SWCNTs with IF-WS$_2$ nanoparticles has been explored. For this purpose, nanocomposites incorporating different SWCNT contents wrapped in PEI as well as hybrid composites reinforced with both types of nanofillers were prepared by conventional melt-blending and hot-press processing techniques. The viscoelastic properties, friction, and wear behavior of the different composites have been compared and the mechanisms of viscosity and friction reduction by the IF-nanoparticles are discussed.

2. EXPERIMENTAL SECTION

2.1. Materials. PEEK (150P) was provided in coarse powder form by Victrex ($d_{2\,°C}$ = 1.32 g/cm^3 $T_g \approx 147$ °C, $T_m \approx 345$ °C). PPS (Fortron 0205B4) was supplied by Ticona in powder form, with an average particle size of 20 μm ($d_{25°C}$ = 1.35 g/cm^3, $T_g \approx 90$ °C, $T_m \approx 280$ °C). The polymers were dried at 100 °C for 14 h and stored in a dry environment before blending. CVD acid purified SWCNTs ($d_{25°C}$ = 2.1 g/cm^3, diameter: 1−2 nm, length: 0.5−2 μm, purity >90%, COOH groups ~2.7%) were purchased from Cheap Tubes Inc. (VT, U.S.A.). Inorganic fullerene-like tungsten disulfide (IF-WS$_2$) nanoparticles (NanoLub, $d_{25°C}$ = 7.50 g/cm^3, average diameter = 80 nm, aspect ratio ~1.4) were provided by Nanomaterials

(Israel). The compatibilizing agent, polyetherimide (PEI 250G) was provided by Sigma-Aldrich in pellet form ($d_{25°C}$ = 1.27 g/cm^3, T_g = 217 °C). The SWCNTs were wrapped by this amorphous polymer in chloroform solution; a detailed description of the wrapping process in liquid medium is given in our previous work.[24] According to TGA analysis, the amount of PEI retained by the SWCNTs was around 7%.

2.2. Preparation of PPS and PEEK-Based Nanocomposites. First, different concentrations of SWCNTs wrapped in PEI were physically mixed with either PPS or PEEK. Each mixture was dispersed in 30 mL of ethanol and ultrasonicated for 30 min at 50 °C. Subsequently, the dispersion was heated in an oven until the solvent was completely removed. Analogously, different weight fractions of wrapped SWCNTs and IF-WS$_2$ were simultaneously mixed with the thermoplastic polymers in ethanol medium. The melt-compounding of all of the mixtures was performed in a Haake Rheocord 90 system operating at 320 or 380 °C for PPS or PEEK, respectively, with a rotor speed of 150 rpm during 20 min. For comparative purposes, reference composites incorporating nonwrapped SWCNTs were also prepared in the same way and are designated by an asterisk (*). Prior to characterization, the nanocomposites were pressed into thin films and annealed for 2 h at 180 °C.

2.3. Characterization Techniques. Atomic force microscopy (AFM) images were obtained on a Multimode Scanning Probe Microscope (Veeco Instruments, Santa Barbara, CA, U.S.A.) equipped with a Nanoscope IVa control system (software versión 6.14r1). An antimony (n) doped silicon-tip cantilever (RTESP, Veeco) with a nominal radius of 8 nm was used, with a resonance frequency of 330 kHz and spring constant of 42 N/m. Samples were prepared as thin films on silicon substrates, and measurements were performed in tapping mode under room temperature conditions and atmospheric environment at a scan rate of 0.5 Hz.

The worn surfaces of the nanocomposites were coated with a 5 nm overlayer of an Au−Pd (80−20) alloy and then observed using a Philips XL 30 scanning electron microscope operating at 25 kV. Transmission electron microscopy (TEM) images were obtained with a Philips Tecnai 20 FEG (LaB$_6$ filament) electron microscope fitted with an EDAX detector operating at 200 kV and with 0.3 nm point-to-point resolution. For TEM analysis, ultrathin sections of the nanocomposites were cut using a diamond knife and a Reichert Ultracut-S ultra-microtome equipped with a FCS cryo-device and placed on copper grids.

Dynamic shear measurements were obtained with a rheometer (AR 1000, TA Instruments) using a parallel plate system (25 mm diameter and 0.75 mm gap). Samples were tested at 360 or 300 °C (for PEEK and PPS based nanocomposites, respectively), under nitrogen conditions, after drying at 100 °C under vacuum to prevent oxidation of the specimens. A dwell time of 10 min was allowed for all experiments to guarantee a uniform melt temperature before starting the measurements. Frequency sweeps from 0.01 to 600 rad/s were performed at a constant strain amplitude of 1%, which is within the linear viscoelastic region for these materials. TA rheometer data analysis software (version VI. 1.76) was used to calculate the storage modulus (G′), loss modulus (G″), and complex viscosity (η*). Rheological tests were carried out in triplicate for each type of nanocomposite.

Pin-on-disk tests were performed on a Microtest MT 400-98 apparatus, using a 6 mm diameter 100Cr6 steel ball like pattern
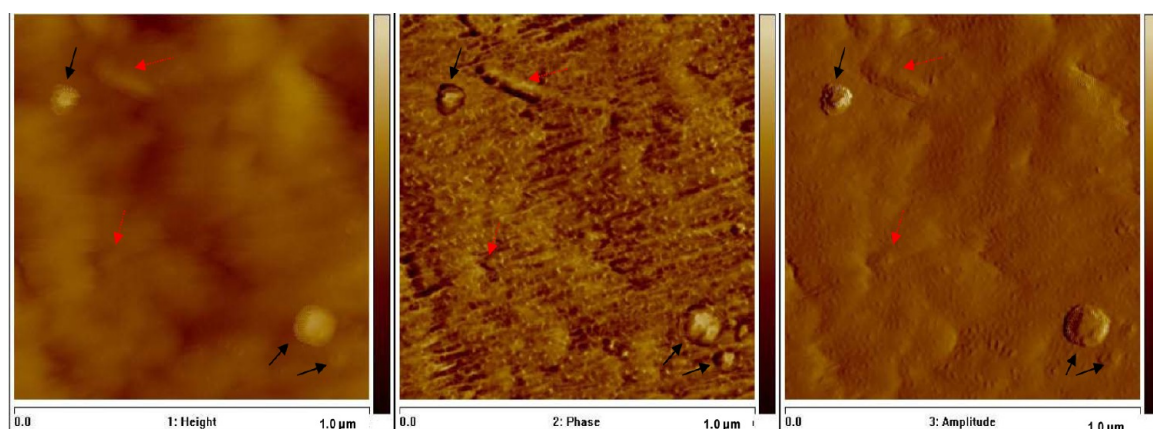
Figure 1. Height (left), phase (middle), and amplitude (right) AFM images of PEEK/SWCNT (0.1 wt %)/IF-WS$_2$ (0.9 wt %) nanocomposite. The black and red arrows point out quasispherical IF-WS$_2$ nanoparticles and SWCNT bundles, respectively.
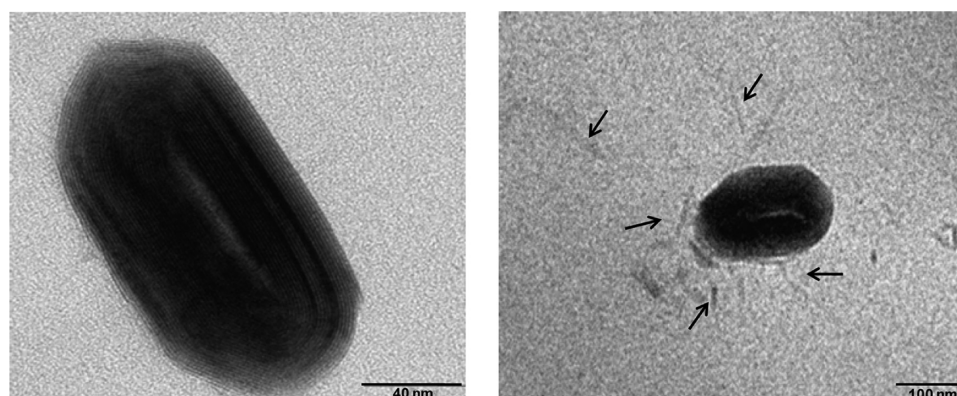
Figure 2. TEM micrographs of PPS/SWCNT (0.5 wt %)/IF-WS$_2$ (1.5 wt %) hybrid nanocomposite. The image on the left shows an ellipsoidal IF-WS$_2$ nanoparticle and that on the right the dispersion of both nanofillers within the PPS matrix. The black arrows point out small SWCNT bundles around a nanoparticle.

slide. Measurements were carried out under a constant load of 5 N at a rotation speed of 375 rpm. The equipment was placed in an isolated box to control the atmosphere conditions, and the experiments were performed under air with a relative humidity of 22 ± 2% and temperature of 24 ± 2 °C. The wear experienced by the flat substrate was determined through the measurement of the wear-track profile by using a profilometer with a resolution of ~10 nm. Each tribological test was repeated three times to ensure reproducibility.

3. RESULTS AND DISCUSSION

3.1. Morphological Observations. The morphology of the nanocomposites was examined by AFM, and representative images of PEEK/SWCNT (0.1 wt %)/IF-WS$_2$ (0.9 wt %) are given in Figure 1. IF-WS$_2$ appeared as either individual nanoparticles or as small aggregates of a few particles, and in all cases these preserved their typical quasi-spherical shape with dimensions ranging from 40 to 180 nm, with a mean value of 80 nm, consistent with the size of the as-received material. The SWCNTs were found to be gathered in loosely entangled bundles, without forming agglomerates, with an average diameter of around 20 nm, similar to that observed for PEEK nanocomposites incorporating solely wrapped or nonwrapped SWCNTs.[24] No preferential location of the nanofillers within the matrix was observed. During the melt-blending process, both IF-WS$_2$ and SWCNTs were randomly dispersed by shear

forces, leading to a homogeneous mixing of both reinforcements with the polymer.

TEM analysis was carried out to obtain further information about the state of dispersion of the nanofillers in the hybrid composites that strongly influences the viscoelastic properties, and typical micrographs of PPS/SWCNT (0.5 wt %)/IF-WS$_2$ (1.5 wt %) are shown in Figure 2. The dark and light areas correspond to the nanofillers and the matrix, respectively. The image at higher magnification (left) presents a closed cage hollow multilayered polyhedral nanoparticle with an ellipsoidal shape and onion-like structure. It is composed of concentric WS$_2$ layers evenly spaced by 6.18 Å. Its hollow nature is reflected by the contrast difference in the core, and the dimension of the hollow void in the center is about half the overall diameter of the nanoparticle. The absence of cracks or voids around the nanoparticles suggests a good IF-WS$_2$-matrix interfacial adhesion. The image at lower magnification (right) shows the distribution of both nanoreinforcements within the matrix. The hybrids display a very uniform spatial distribution of the SWCNTs, ascribed to the presence of the nanoparticles that possess lubricant character and reduce the viscosity of the matrix, as will be discussed in a following section. The SWCNTs are randomly dispersed with no preferred alignment, showing a low degree of waviness. It is found that the ends of some SWCNTs are close to the nanoparticle surfaces, suggesting the formation of a unique network that combines both nanofillers. A jammed and well dispersed IF-WS$_2$/

SWCNT network is required to attain the rheological percolation.

3.2. Rheological Behavior. The study of the rheological behavior is crucial for understanding the structure—property relationships of polymer composites and optimizing their processing conditions. Therefore, the viscoelastic properties of the different nanocomposites in the molten state were investigated, and the frequency (ω) dependence of the storage modulus (G′) and loss modulus (G″) of compatibilized PPS/SWCNT nanocomposites at a temperature of 300 °C is depicted in Figure 3. For comparative purposes, the curves for
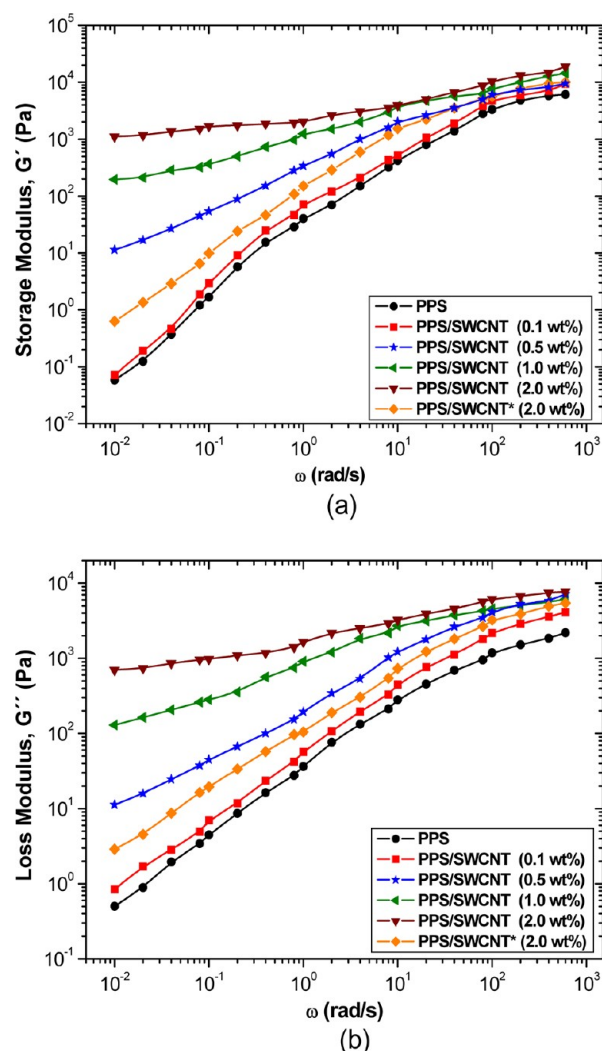
Figure 3. Storage modulus G′ (a) and loss modulus G″ (b) as a function of frequency ω, at 300 °C, for neat PPS and compatibilized nanocomposites with various SWCNT contents. The asterisk indicates the noncompatibilized sample.

neat PPS and the binary sample incorporating nonwrapped SWCNTs are also included in the plot. It can be observed that the magnitude of both moduli rises with frequency, the increment in G′ being larger than that for G″. Moreover, although both parameters increase with SWCNT loading, the slope of the curves decreases. The influence of the SWCNTs is more pronounced in the low-frequency range, and the differences between the composite moduli and those of the matrix weaken with increasing frequency due to a shear thinning effect. The low-frequency power-law dependence of G′

and G″ versus ω is presented in Table 1. Neat PPS exhibits typical homopolymer-like terminal behavior that approximately obeys the expected scaling law predicted by the theory of linear viscoelasticity,[25] G′ ≈ ω^2 and G″ ≈ ω, indicating that the polymer chains are fully relaxed. However, in the SWCNT-reinforced composites, the power-law exponents of G′ and G″ deviate from the theoretical dependence, decreasing monotonically with increasing nanotube content, from 1.82 to 0.23 and 0.95 to 0.20, respectively. For SWCNT loadings ≥0.5 wt %, the terminal behavior disappears, tending to a plateau like-regime that indicates a transition from liquid-like to solid-like viscoelastic behavior. This nonterminal behavior is attributed to the formation of a SWCNT network that restricts the long-range motion of the polymer chains. Similar observations have been reported for different thermoplastic nanocomposites containing CNTs[5,8] or clays.[26] At high frequencies, the effect of the SWCNTs on both moduli is weaker, suggesting that these slightly influence the short-range dynamics of the PPS chains, particularly at the length scales comparable to or less than an entanglement length.

It has been reported[5] that the degree of CNT dispersion strongly influences the viscoelastic properties of CNT-reinforced polymer nanocomposites. Smaller low-frequency slopes of G′ versus ω and higher storage modulus values are associated with a more homogeneous nanofiller distribution. In the terminal zone, the reference sample with 2.0 wt % SWCNT loading shows a considerably higher slope, around a 5-fold increase compared to the compatibilized composite with the same amount of wrapped SWCNTs, and exhibits almost 3 orders of magnitude lower values of G′. Moreover, terminal behavior is manifested, as in the case of neat PPS. This is consistent with the observations from SEM analysis,[20] which revealed poorer nanotube distribution for the noncompatibilized nanocomposites. This reference sample has discrete nanotube-rich domains rather than a homogeneous CNT network; hence, the polymer chains flow independently of the SWCNTs, and their motion should be very similar to those of neat PPS.

The complex shear viscosity (η) as a function of ω for neat PPS and the SWCNT-reinforced nanocomposites is shown in Figure 4. The neat polymer, the noncompatibilized nanocomposite, and that incorporating 0.1 wt % wrapped SWCNTs remain essentially Newtonian, whereas the rest of the nanocomposites exhibit strong shear thinning behavior and η decreases progressively with increasing frequency. This behavior has been attributed to the orientation of the rigid molecular chains in the composites when exposed to shear forces.[27] The complex viscosity of PPS rises with increasing SWCNT concentration, and the extent of this change is more significant at low frequencies, around 3 orders of magnitude for the compatibilized nanocomposite with 2.0 wt % loading. Moreover, for SWCNT contents higher than 0.1 wt %, the Newtonian plateau disappears, and the low-frequency slope increases with CNT concentration. Thus, for the nanocomposite with the highest loading the viscosity curve is almost linear over the whole frequency range. The aforementioned results are in good agreement with both theoretical predictions[28] and experimental observations[5,8,27] for CNT-reinforced polymer composites. Regarding the noncompatibilized sample, the increase in η is less than 1 order of magnitude in the terminal zone. The significantly smaller increment compared with the nanocomposite incorporating the same amount of SWCNTs wrapped in PEI is attributed to a

Table 1. Low-Frequency Slopes of G′ and G″ vs ω and Fitting Results from Power-Law Relations of G′ and η vs SWCNT Loading for PPS and PEEK-Based Nanocomposites

| matrix	SWCNT (wt %)	IF-WS$_2$ (wt %)	slope of G′	slope of G″	$m_{c,G'}$ (wt %)	$m_{c,\eta}$ (wt %)	$\beta_{c,G'}$	$\beta_{c,\eta}$
PPS			1.82	0.95	0.29	0.33	1.82	1.60
	0.1		1.79	0.90				
	0.5		0.84	0.69				
	1.0		0.36	0.35				
	2.0		0.23	0.20				
	2.0^a		1.27	0.78				
PEEK			1.96	0.98	0.07	0.08	1.49	1.07
	0.1		0.90	0.75				
	0.5		0.45	0.38				
	1.0		0.34	0.29				
	1.0^a		1.32	0.82				
PPS	0.5	1.5	0.61	0.43	0.25	0.38	2.03	1.73
	1.0	1.0	0.25	0.22				
	1.5	0.5	0.13	0.11				
PEEK	0.1	0.9	0.79	0.57	0.07	0.09	1.54	1.04
	0.5	0.5	0.38	0.36				
	0.9	0.1	0.22	0.14				

^{a}Nonwrapped SWCNTs.
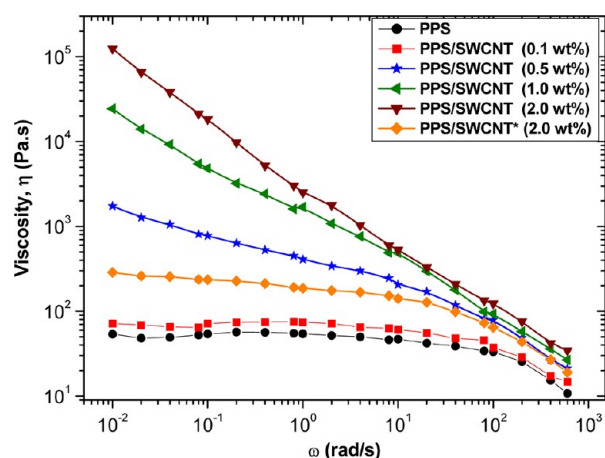
Figure 4. Complex viscosity η of PPS and the SWCNT-reinforced nanocomposites versus ω at 300 °C.

compatibilization effect, where polar groups of the PEI chains can form hydrogen bonds with the oxygen groups located on the surface of the acid-treated SWCNTs; likewise, its phenyl and imidazole moieties can interact with both PPS and SWCNTs through $\pi-\pi$ stacking. Therefore, the presence of the compatibilizer improves the dispersion of the SWCNTs in the matrix generating a larger η increment.

Figure 5a shows the evolution of G′ as a function of ω for neat PEEK, the reference noncompatibilized sample and compatibilized nanocomposites incorporating different SWCNT loadings. An analogous behavior was found for the frequency dependence of G″ (data not shown), and the trends observed were qualitatively similar to those reported above for PPS composites. Neat PEEK has a typical terminal regime with scaling properties of G′ $\approx \omega^{1.96}$ and G″ $\approx \omega^{0.98}$ (Table 1). All of the compatibilized nanocomposites deviate from this behavior, and the dependence of G′ and G″ on ω weakens with increasing nanotube concentration. Again, the differences between the moduli of the composites and the matrix become smaller as the frequency is increased. Comparing the same frequency and SWCNT content, these nanocomposites display higher G′
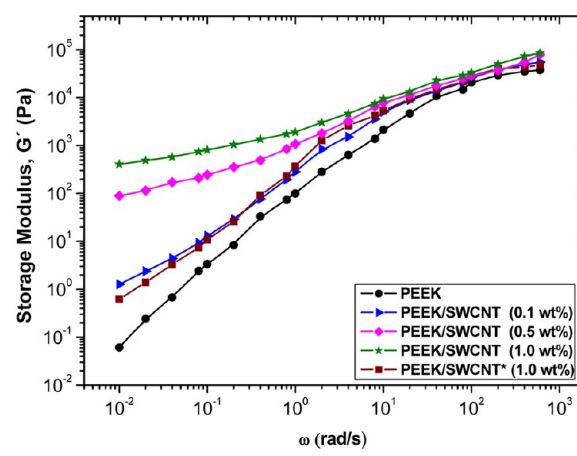
(a)
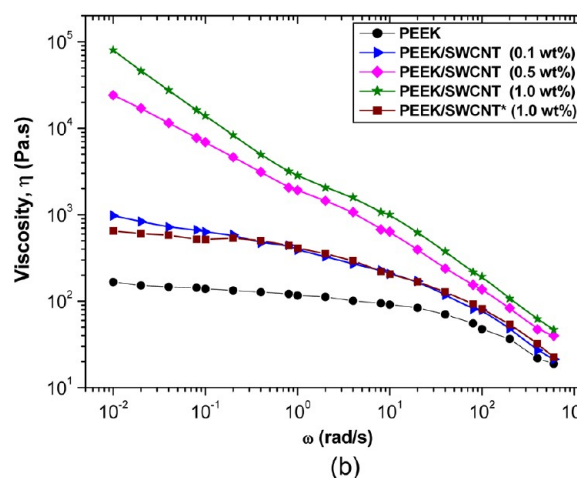
(b)

Figure 5. Storage modulus (a) and complex viscosity (b) versus ω, at 360 °C, for neat PEEK and nanocomposites with different loadings of SWCNTs wrapped in PEI. The noncompatibilized nanocomposite is designated by an asterisk.

values than those based on a PPS matrix. Moreover, their low-frequency slopes of G′ and G″ are higher, suggesting improved

SWCNT dispersion. This fact may be related to different mechanisms of compatibilization. PEI is an amorphous polymer miscible with and structurally similar to PEEK,[24] whereas it is immiscible with PPS in the whole composition range leading to binary phase morphologies.[29] As mentioned above, the compatibilization in PPS nanocomposites is based solely on PEI-PPS and PEI-SWCNT interactions, whereas in the case of PEEK an intimate mixture between the two polymers is also achieved that boosts the matrix-SWCNT interactions. Therefore, the miscibility and higher affinity of PEI for PEEK results in a more homogeneous SWCNT distribution within the matrix that is reflected in higher moduli. On the other hand, among the PEEK based nanocomposites, the binary reference sample with 1.0 wt % loading shows the highest low-frequency slope of G′ and the lowest G′ values, which is clearly indicative of poorer nanotube dispersion.

Regarding the melt viscosity of PEEK/SWCNT nanocomposites versus frequency, Figure 5b, the trends found are also analogous to those described previously for PPS nanocomposites. The value of η for PEEK and the non-compatibilized sample changes slightly with ω, whereas the compatibilized composites display shear thinning behavior and a steep slope at low frequencies, particularly for SWCNT loadings ≥ 0.5 wt %. Furthermore, their viscosities are orders of magnitude higher than that of neat PEEK in the terminal zone. For the same SWCNT concentration, these composites show a stronger increase in viscosity compared with those with a PPS matrix, most likely due to their improved SWCNT dispersion.

It can be observed from Figures 3, 4 and 5 that both η and G′ experience a sharp increase at a critical SWCNT concentration that is known as the rheological percolation threshold. This sudden increase is related to the formation of a CNT network interpenetrating the matrix molecular chains. At lower concentrations, the SWCNTs only restrict the local mobility of individual polymer chains. However, at the percolation threshold tube−tube interactions begin to dominate over polymer-SWCNT interactions and the restrictions extend throughout the composite, resulting in strong increases in G′ and η. To determine the percolation thresholds for PPS and PEEK nanocomposites, two power-law relations can be used:[27]

$$G' \approx (m - m_{c,G'})^{\beta_{c,G'}} \qquad (1)$$

$$\eta \approx (m - m_{c,\eta})^{\beta_{c,\eta}} \qquad (2)$$

where m is the SWCNT loading, $m_{c,G'}$ and $m_{c,\eta}$ are rheological percolation thresholds, and $\beta_{c,G'}$ and $\beta_{c,\eta}$ are critical exponents. G′ and η for both types of composites at a fixed frequency of 0.04 rad/s are plotted as a function of SWCNT content in Figure 6, and the best-fit results to eqs 1 and 2 are included in Table 1. As an example, the insets of Figure 6 present the log−log plot of both parameters versus m-m_c for PPS/SWCNT composites. In this system, $m_{c,G'}$ and $m_{c,\eta}$ are quite similar (0.29 and 0.33 wt %, respectively), and significantly higher than those obtained for PEEK/SWCNT nanocomposites (0.07 and 0.08 wt %, respectively), which exhibit sharper increases in viscosity and modulus. The lower percolation threshold obtained for PEEK based nanocomposites indicates improved SWCNT dispersion, ascribed to the miscibility and higher structural affinity of this polymer matrix with the compatibilizing agent, as discussed earlier. Previous studies on MWCNT-reinforced polycarbonate (PC)[8] and poly(ethylene terephthalate) (PET)[27] nanocomposites found m_c values of about 0.5 wt %.
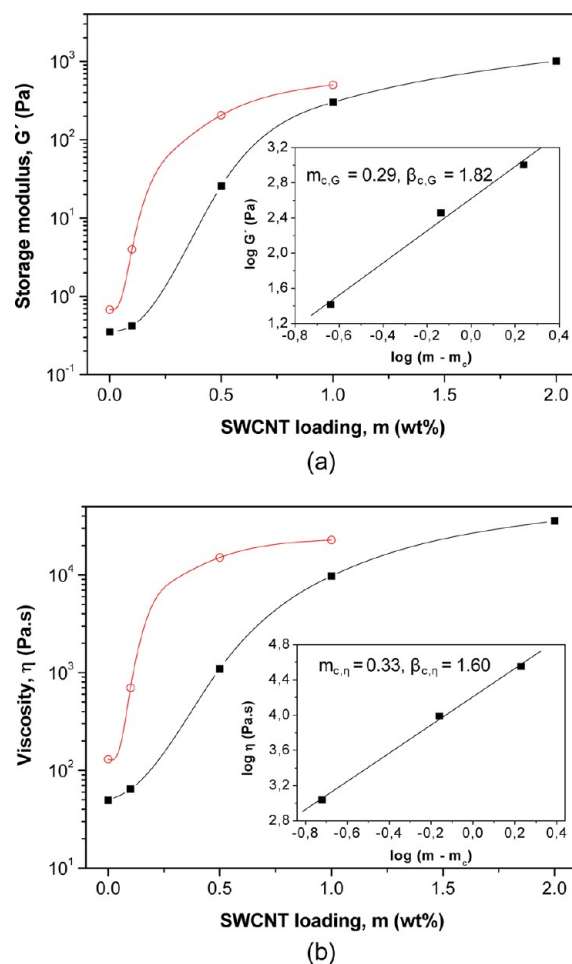
Figure 6. Storage modulus (a) and complex viscosity (b) of compatibilized PPS/SWCNT (solid symbols) and PEEK/SWCNT nanocomposites (open symbols) as a function of SWCNT loading at a fixed frequency of 0.04 rad/s. The insets show the log−log plot of G′ and η versus $m - m_c$ for PPS nanocomposites, and the straight lines are fits to the power-law relations (eqs 1 and 2).

The critical concentrations observed in this work are found to be considerably lower than reported results, which can be attributed to the enhanced filler dispersion and stronger CNT-matrix interfacial bonding due to the presence of the compatibilizer, combined with the higher aspect ratio of SWCNTs compared to MWCNTs. Regarding the critical exponents, $\beta_{c,G'}$ is systematically higher than $\beta_{c,\eta}$, since the variation in viscosity at the threshold is smaller than the change in modulus. Similarly, the values obtained for PPS/SWCNT nanocomposites are higher than those fitted for PEEK based nanocomposites, due to the larger magnitude of the change in G′ and η at the threshold.

Generally, the formation of a CNT network affects both the rheological and electrical properties in a related manner.[5] Therefore, it is interesting to compare $m_{c,G'}$ with the electrical percolation threshold ($m_{c,\sigma}$) found for these nanocomposites.[20,24] The values of $m_{c,\sigma}$ are around 0.1 and 0.45 wt % for SWCNT-reinforced PEEK and PPS nanocomposites, respectively, slightly higher than those obtained from rheology measurements. This fact has also been observed in other polymer/CNT systems such as PET/MWCNT[27] and PC/MWCNT[8] nanocomposites, and explained in terms of the different tube−tube distances required for rheological or

electrical percolation.[5] It is assumed that for the latter phenomenon the CNTs need to be sufficiently adjacent to allow electron hopping or tunnelling (intertube distance ≤5 nm). However, when the gap between CNTs is smaller than the radius of gyration of the matrix chains, typically dozens of nanometers, the CNT network can effectively restrict polymer chain mobility. Consequently, more tubes are required to reach the electrical conductivity threshold. Moreover, the network consists of a random mixture of metallic and semiconducting SWCNTs, and the nonmetallic tubes only slightly contribute to the electrical conductivity, albeit restrain chain motion.

The rheological properties in the molten state of hybrids incorporating both IF-WS$_2$ nanoparticles and SWCNTs were also investigated, and representative curves of G′ and η versus ω for PPS and PEEK based nanocomposites are displayed in Figures 7 and 8, respectively. As can be observed, the trends are
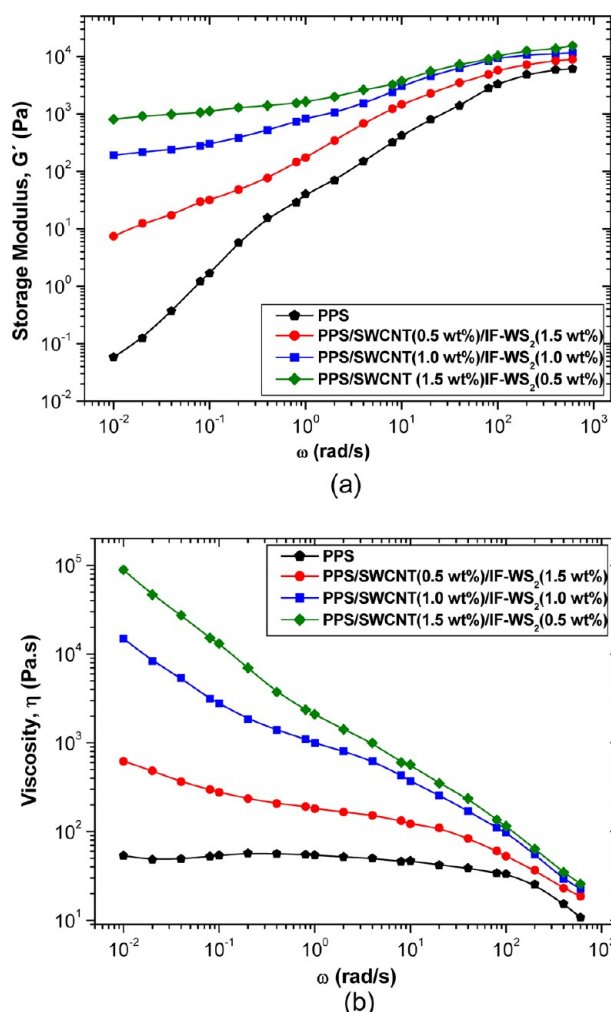
Figure 7. Storage modulus (a) and complex viscosity (b) versus ω in the molten state for PPS based hybrid nanocomposites with different SWCNT and IF-WS$_2$ loadings.

similar to those found for the compatibilized SWCNT-reinforced composites, showing nonterminal behavior. However, in the low-frequency region, the hybrids exhibit lower moduli values (Figures 7a and 8a), and the extent of the decrease in G′ is strongly dependent on the composition. Thus, at a frequency of 0.04 rad/s, PEEK/SWCNT (0.1 wt %)/IF-WS$_2$ (0.9 wt %) shows about 40% lower modulus than the
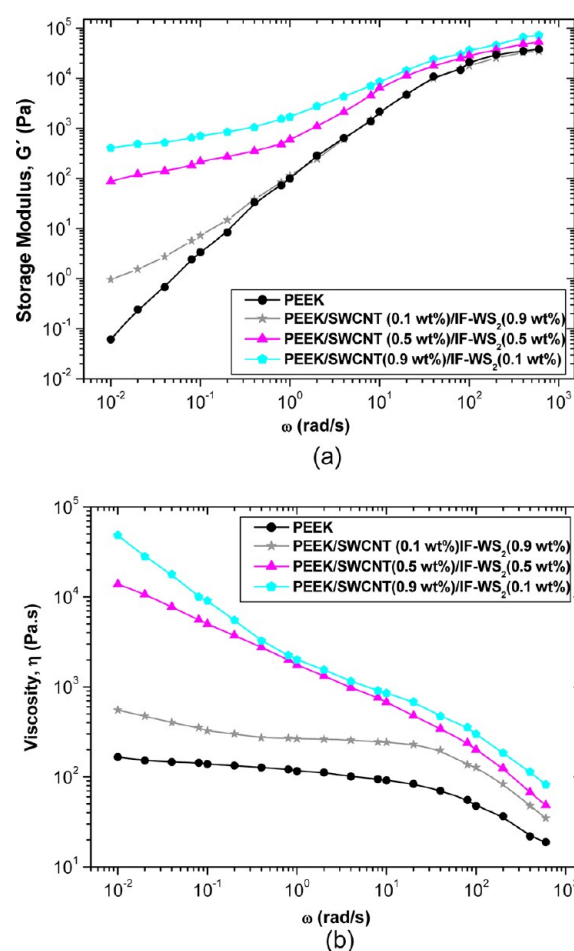
Figure 8. Storage modulus (a) and complex viscosity (b) as a function of ω for PEEK/SWCNT/IF-WS$_2$ hybrid nanocomposites.

composite reinforced solely with the same amount of wrapped SWCNTs, whereas in the case of PEEK/SWCNT (0.9 wt %)/IF-WS$_2$ (0.1 wt %) the reduction is only around 4%. This drop in G′ is closely related to the decrease in viscosity caused by the nanoparticles, as shown in Figures 7b and 8b. On the other hand, the low-frequency slopes of G′ and G″ for the different hybrids are listed in Table 1; it is found that these values are lower than those of the corresponding PPS/SWCNT or PEEK/SWCNT nanocomposites with the same nanotube content, which can be associated with better SWCNT dispersion. This is consistent with the observations from TEM analysis that revealed a very homogeneous distribution of the SWCNTs in the presence of the IF-WS$_2$ nanoparticles.

The viscosity of all the hybrids decreases with increasing frequency, showing non-Newtonian behavior (Figures 7b and 8b). As mentioned above, they exhibit lower η compared with the composites including solely SWCNTs, and this reduction is more pronounced in the low-frequency range, becoming more significant with increasing nanoparticle concentration. For example, at ω = 0.04 rad/s, the viscosity of PPS/SWCNT (0.5 wt %) dropped by about 60% when 1.5 wt % IF-WS$_2$ were added. An analogous behavior of melt viscosity reduction has been reported for silica-reinforced poly(ethylene 2,6-naphthalate) (PEN)[30] and PET[31] nanocomposites. The drop in η is ascribed to slippage between the polymer and the quasi-spherical nanoparticles with a smooth nonporous surface, which serve as ball-bearing agents, reducing the coefficient of friction

as demonstrated by tribological tests and facilitating the flow of the polymer chains. This confirms that the IF-WS$_2$ acted as a lubricant when the polymer/nanofiller mixture was exposed to high shear forces and heat during the melt-blending process, promoting a more uniform SWCNT dispersion within the matrix. Another factor that could have an influence on the decrease in viscosity is the change in free volume due to the addition of the IF-WS$_2$. Assuming that an excluded volume layer of thickness Δ exists around each nanoparticle, the fractional free volume (f) within the polymer matrix is increased by $\sim 3V_f\Delta/a$,[32] where V_f is the particle volume fraction and a is the average radius. Thus, taking $V_f = 0.1$ and $\Delta = 0.1$ nm, the increase in free volume at the melt temperature would be very small (~ 0.0007). Therefore, the effect of free volume on the viscosity is expected to be negligible. It is worth mentioning that the phenomenon of viscosity reduction observed when IF-WS$_2$ are added to PPS or PEEK melts is in contrast with the typical behavior reported for polymer/nanoparticle nanocomposites,[33] where η rises with increasing nanofiller loading. The discrepancy is believed to be caused by the different geometric shape and structure of the nanoparticles.

The percolation thresholds and critical exponents for the hybrid composites were also estimated using eqs 1 and 2, and the results are presented in Table 1. Interestingly, the values of $m_{c,G'}$ for the hybrids are slightly lower than those of the corresponding nanocomposites reinforced solely with wrapped SWCNTs, whereas $m_{c,\eta}$ values are a little higher. Moreover, $\beta_{c,G'}$ and $\beta_{c,\eta}$ are found to be similar or slightly higher. Therefore, it can be concluded that both types of systems percolate approximately at the same SWCNT concentration. Despite the presence of the IF-WS$_2$ leads to a more homogeneous SWCNT dispersion that is expected to yield a rheological percolation at lower concentration, it could also modify the interconnectivity of the SWCNTs within the matrix that would compensate for the improvement in dispersion.

3.3. Tribological Properties. To confirm the lubricant effect of the IF-WS$_2$, the coefficient of friction (μ) and wear rate (k) of the hybrids were measured and compared with those of composites incorporating solely SWCNTs. The results for PPS based nanocomposites are plotted in Figure 9. Neat PPS exhibits a high μ of around 0.4 that falls by $\sim 9\%$ with the addition of 2.0 wt % nonwrapped SWCNTs (Figure 9a). This small decrease could be attributed to the high strength of the SWCNTs that restrain the scuffing and adhesion of the matrix during the sliding process providing a much better resistance than the neat polymer, combined with the increase in thermal conductivity that lowers the temperature in the sliding contact. Moreover, the SWCNTs act as a barrier and prevent large-scale fragmentation of the matrix. However, all the nanocomposites incorporating SWCNTs wrapped in PEI show similar μ to that of the neat matrix, probably due to the polymer coating, since the compatibilizing agent possesses almost the same μ as PPS.[34] Regarding the hybrids, a significant drop in μ is observed compared to similar nanocomposites without nanoparticles, and the extent of the decrease rises with increasing IF-WS$_2$ loading. Thus, the largest reduction ($\sim 33\%$) corresponds to PPS/SWCNT (0.5 wt %)/IF-WS$_2$ (1.5 wt %).

Figure 9b shows that the wear rate of noncompatibilized PPS/SWCNT (2.0 wt %) is considerably lower than that of the neat matrix (more than a 3-fold decrease), whereas for the corresponding compatibilized sample the drop in k is around 2-fold. The larger improvement in wear resistance in the former nanocomposite is ascribed to the SWCNTs exposed to the

(a)

(b)
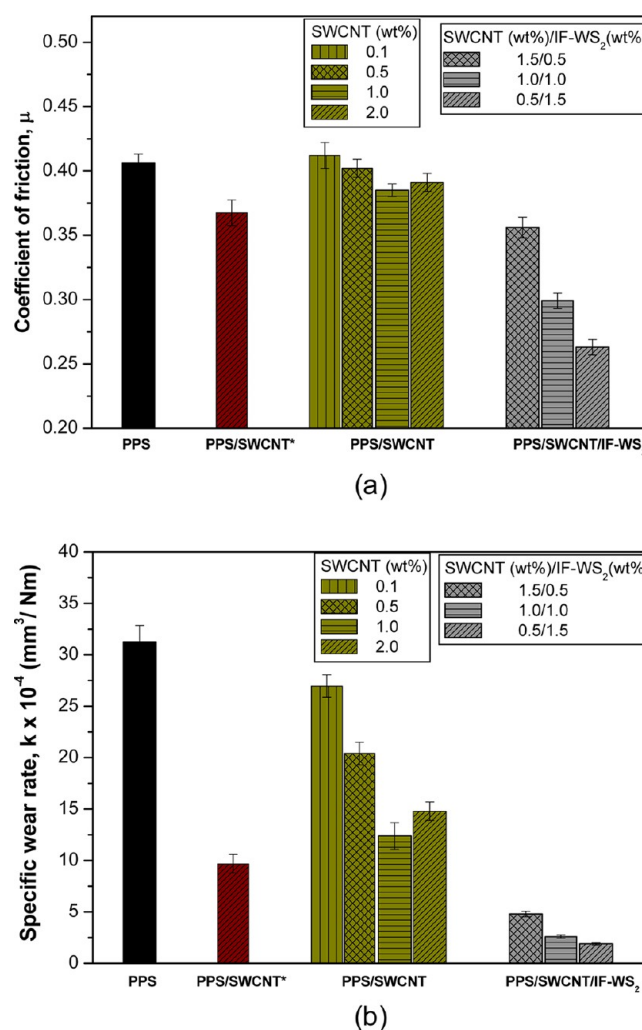
Figure 9. Coefficient of friction (a) and wear rate (b) for PPS based nanocomposites and the neat polymer.

sliding interface that effectively protected the matrix. Although the addition of the compatibilizer improves the SWCNT dispersion and the mechanical properties of the composites (i.e., modulus and impact strength),[20] facts that are expected to result in improved tribological properties, it reduces the lubricant capability of the nanotubes that is reflected in a smaller decrease in both μ and k. Focusing on the influence of the SWCNT loading, it is found that k reaches a minimum at 1.0 wt % wrapped SWCNTs and then increases slightly despite the higher stiffness of the nanocomposite with 2.0 wt % loading. As revealed in previous works,[20,24] the presence of SWCNTs decreases the elongation at break and toughness of the composite material, these reductions becoming more drastic at concentrations >1.0 wt %, significantly increasing the composite brittleness, hence decreasing the wear resistance. A similar trend has been reported for PPS/Al$_2$O$_3$ nano-composites,[35] where k passed through a minimum at an optimum loading of 2 vol. %, attributed to the formation of small particle aggregates that hinder the formation of a continuous transfer film on the counter surface. With regard to the hybrids, a progressive reduction in this parameter is found with increasing IF-WS$_2$ concentration, decreasing for the sample with 1.5 wt % loading by approximately a factor of 16 in relation to that of the neat matrix, or around an 8-fold decrease

compared to a similar nanocomposite without nanoparticles. These excellent tribological properties can be ascribed to the high stiffness and strength of the IF-WS$_2$ nanoparticles, their chemical inertness and hollow cage structure that provides certain elasticity and lubrication capability, combined with a synergistic effect arising from the presence of the two nanofillers. Rapport et al.[36] have proposed a rolling mechanism for these nanoparticles where the IF-WS$_2$ act as a type of ball-bearing component, meaning that they roll rather than slide between the surfaces, effectively reducing the shear stress, coefficient of friction and contact temperature. Moreover, the nanoparticles serve as spacers, preventing the contact between the asperities of the composite surface and the steel counterpart. Nevertheless, the main friction mechanism is expected to be the transfer of pristine IF-WS$_2$ or exfoliated external layers of the hollow nanoparticles from the surface of the sample to the surface of the counterpart, reducing both the sliding friction and wear rate. The gradual release of WS$_2$ sheets and their transfer to the contact surfaces is probably the most important action under severe contact conditions when the distance between the rubbed surfaces is smaller than the size of the nanoparticles.

The influence of the IF-WS$_2$ on the tribological behavior of PEEK/SWCNT nanocomposites was also investigated, and the experimental k and μ data for the different composites are compared in Figure 10. The addition of increasing SWCNT loadings wrapped in PEI to the PEEK matrix leads to a progressive decrease in both parameters, particularly in the wear rate, which drops nearly 2-fold for the compatibilized nanocomposite with 1.0 wt %. Comparing the same SWCNT content, the improvement in wear resistance is larger for these nanocomposites in relation to those based on a PPS matrix and can be ascribed to their higher hardness and stiffness combined with their improved SWCNT dispersion, since a more homogeneous distribution results in a thinner and more uniform transfer film.[37] Nevertheless, the noncompatibilized sample incorporating 1.0 wt % loading displays again lower k and μ than the corresponding nanocomposite with the same amount of wrapped SWCNTs, thereby confirming that polymer wrapping is not beneficial for enhancing the tribological performance of these systems. With regard to the hybrids, a significant decrease in both parameters is observed compared to the samples reinforced solely with SWCNTs, following similar trend to that described above for PPS based composites. The largest drops are encountered for the hybrid with the highest IF-WS$_2$ loading, where k and μ decreased by factors of 14 and 1.5, respectively. As mentioned earlier, the excellent wear behavior of the hybrids can be ascribed to the outstanding lubricant properties of these nanoparticles together with a synergistic effect of both nanofillers on the enhancement of the sliding wear resistance. Finally, it is worth noting that the hybrids studied in this work possess considerably improved tribological performance compared with PEEK or PPS based composites incorporating nanoscale inorganic fillers such as Al$_2$O$_3$,[35,38] CuO,[39] or ZrO$_2$,[40] where the coefficient of friction remained similar to that of the polymer, and the wear rate only decreased between one and 3-fold.

To obtain more information about the wear mechanism of the composites, their worn surfaces were observed by SEM, and typical micrographs of PEEK/SWCNT (0.1 wt %) and PEEK/SWCNT (0.1 wt %)/IF-WS$_2$ (0.9 wt %) are displayed in Figure 11. Microcracks, ploughing, and some scuffing can be observed on the surface of the former composite (Figure 11a), and
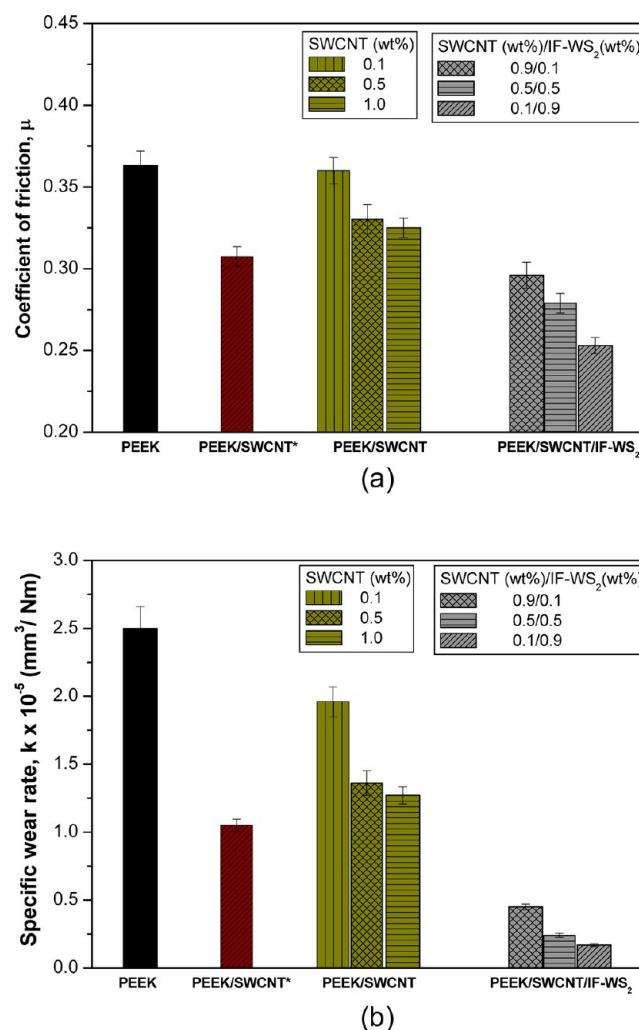
Figure 10. Comparison of the coefficient of friction (a) and wear rate (b) for PEEK and the corresponding nanocomposites.

adhesive wear seems to be the dominant mechanism. A large amount of debris is also found due to the scuffing of the hard asperities on the steel counterpart. In contrast, the hybrid sample presents a much smoother surface (Figure 11b), without signs of ploughing, scuffing or cracking and a very small amount of debris. Clearly the incorporation of nanoparticles inhibits the adhesive wear and increases the surface hardness that provides resistance against the embedding of the hard asperities on the counterpart surface, and consequently scuffing is abated.

4. CONCLUSIONS

The rheological and tribological properties of melt-extruded PPS and PEEK based nanocomposites incorporating PEI-wrapped SWCNTs were analyzed as a function of the nanofiller loading, and compared with the behavior of hybrid composites incorporating SWCNTs and IF-WS$_2$. AFM and TEM demonstrated a very homogeneous dispersion of both nanofillers within the matrices. The complex viscosity η and both moduli (G' and G″) increased monotonically with increasing SWCNT content. At loadings $\geq$0.5 wt %, composites showed a strong shear thinning behavior with a plateau in both moduli at low frequencies, indicating the formation of a percolated SWCNT network. The addition of increasing IF-WS$_2$ contents
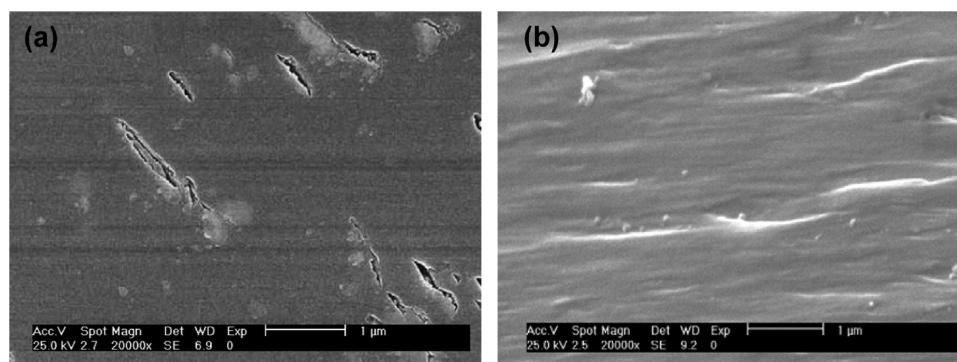
Figure 11. SEM micrographs from worn surfaces of (a) PEEK/SWCNT (0.1 wt %) and (b) PEEK/SWCNT (0.1 wt %)/IF-WS$_2$ (0.9 wt %) nanocomposites.

resulted in a gradual decrease in η and G′, attributed to the slippage between the polymer and the quasi-spherical nanoparticles. By plotting G′ and η vs SWCNT loading and fitting to power-law relations, the percolation thresholds of PPS and PEEK based nanocomposites were determined to be ∼0.3 and 0.08 wt %, respectively. The lower rheological percolation of PEEK nanocomposites is ascribed to their improved SWCNT dispersion, since PEI possesses higher structural affinity with PEEK. The coefficient of friction of the matrices slightly decreased with the addition of SWCNTs, whereas a significant drop was found in the wear rate. Composites incorporating both nanofillers displayed considerably improved wear resistance, ascribed to the high stiffness and strength of the IF-WS$_2$, their chemical inertness and hollow cage structure that provides certain elasticity and lubrication capability, combined with a synergistic effect. The experimental results confirm that the addition of small amounts of IF-WS$_2$ nanoparticles is a highly effective method to improve the processing as well as the tribological and rheological performance of CNT-reinforced thermoplastic nanocomposites such as those based on PPS or PEEK.

■ AUTHOR INFORMATION

Corresponding Author
*E-mail: adiez@ictp.csic.es. Tel: + 34 91 562290. Fax: +34 91 5644853.

Notes
The authors declare no competing financial interest.

■ ACKNOWLEDGMENTS

■ REFERENCES

(1) Spitalsky, Z.; Tasis, D.; Papagelis, K.; Galiotis, C. *Prog. Polym. Sci.* **2010**, *35*, 357−401.
(2) Sung, Y. T.; Han, M. S.; Song, K. H.; Jung, J. W.; Lee, H. S.; Kum, C. K.; Joo, J.; Kim, W. N. *Polymer* **2006**, *47*, 4434−4439.
(3) Diez-Pascual, A. M.; Naffakh, M.; Gómez, M. A.; Marco, C.; Ellis, G.; Martínez, M. T.; Ansón, A.; González-Domínguez, J. M.; Martínez-Rubi, Y.; Simard, B. *Carbon* **2009**, *47*, 3079−3090.

(4) Barraza, H. J.; Pompeo, F.; ÓRea, E. A.; Resasco, D. E. *Nano Lett.* **2002**, *2*, 797−802.
(5) Du, F.; Scogna, R. C.; Zhou, W.; Brand, S.; Fischer, J. E.; Winey, K. I. *Macromolecules* **2004**, *37*, 9048−9055.
(6) Bangarusamplath, D. S.; Ruckdäschel, H.; Altstädt, V.; Sandler, J. K. W.; Garray, D.; Shaffer, M. S. P. *Polymer* **2009**, *50*, 5803−5811.
(7) Han, S. H.; Lee, K. Y.; Lee, S. H.; Yun, C. H.; Kim, W. N. *Chem. Eng. Sci.* **2009**, *64*, 4649−4656.
(8) Pötschke, P.; Fornes, T. D.; Paul, D. R. *Polymer* **2002**, *43*, 3247−3255.
(9) Meincke, O.; Kaempfer, D.; Weickmann, H.; Friedrich, C.; Vathauer, M.; Warth, H. *Polymer* **2004**, *45*, 739−748.
(10) Yu, L.; Yang, S.; Liu, W.; Xue, Q. *Polym. Eng. Sci.* **2000**, *40*, 1825−1832.
(11) Cho, M. H.; Bahadur, S. *Tribol. Lett.* **2007**, *25*, 237−245.
(12) Kuo, M. C.; Tsai, C. M.; Huang, J. C.; Chen, M. *Mater. Chem. Phys.* **2005**, *90*, 185−195.
(13) Margulis, L.; Salitra, G.; Tenne, R.; Talianker, M. *Nature* **1993**, *365*, 113−114.
(14) Hou, X.; Shan, C. X.; Choy, K.-L. *Surf. Coat. Technol.* **2008**, *202*, 2287−2291.
(15) Svahn, F.; Csillag, S. *Tribol. Lett.* **2011**, *41*, 387−393.
(16) Diez-Pascual, A. M.; Ashrafi, B.; Naffakh, M.; González-Domínguez, J. M.; Johnston, A; Simard, B.; Martínez, M. T.; Gómez, M. A. *Carbon* **2011**, *49*, 2817−2833.
(17) Werner, P.; Altstädt, V.; Jaskulka, R.; Jacobs, O.; Sandler, J. K. W.; Shaffer, M. S. P. *Wear* **2004**, *257*, 1006−1014.
(18) Naffakh, M.; Diez-Pascual, A. M.; Marco, C.; Gómez, M. A.; Jímenez, I. *J. Phys. Chem. B* **2010**, *114*, 11444−11453.
(19) Naffakh, M.; Marco, C.; Gómez, M. A. J; Jiménez, I. *J. Phys. Chem. B* **2009**, *113*, 10104−10111.
(20) Diez-Pascual, A. M.; Naffakh, M.; Marco, C.; Ellis, G. *Compos. Part A* **2012**, *43*, 603−612.
(21) Diez-Pascual, A. M.; Naffakh, M.; Gómez-Fatou, M. A. *Mater. Chem. Phys.* **2011**, *130*, 126−133.
(22) Naffakh, M.; Diez-Pascual, A. M.; Gómez-Fatou, M. A. *J. Mater. Chem.* **2011**, *21*, 7425−7433.
(23) Naffakh, M.; Diez-Pascual, A. M.; Marco, C.; Ellis, G. *J. Mater. Chem.* **2012**, *22*, 1418−1425.
(24) Diez-Pascual, A. M.; Naffakh, M.; Gómez, M. A.; Marco, C.; Ellis, G.; Martínez, M. T.; Ansón, A.; González-Domínguez, J. M.; Martínez-Rubi, Y.; Simard, B.; et al. *Nanotechnology* **2009**, *20*, 315707−315720.
(25) Ferry, J. D. *Viscoelastic Properties of Polymers*, 3rd ed.; John Wiley & Sons: New York, 1980.
(26) Ray, S. S. *Prog. Polym. Sci.* **2003**, *28*, 1539−1641.
(27) Hu, G.; Zhao, C.; Zhang, S.; Yang, M. *Polymer* **2006**, *47*, 480−488.
(28) Mutel, A. T.; Camel, M. R. Two Phase Polymer Systems. In Utracki, L. A., Ed.; *Rheological properties of fibre-reinforced polymer melts*; Carl Hanser: Munich, 1991; Vol. *12*, pp 305−331.
(29) Akhtar, S.; White, J. L. *Polym. Eng. Sci.* **1991**, *31*, 84−91.

(30) Kim, S. H.; Ahn, S. H.; Hirai, T. *Polymer* **2003**, *44*, 5625−5634.

(31) Im, S. S.; Chung, S. C.; Hahm, W. G.; Oh, S. G. *Macromol. Res.* **2002**, *10*, 221−229.

(32) Tuteja, T.; Mackay, M. E.; Hawker, C. J.; Van Horn, B. *Macromolecules* **2005**, *38*, 8000−8011.

(33) Knauert, S. T.; Douglas, J. F.; Starr, F. W. *J. Polym. Sci.; Part B: Polym. Phys.* **2007**, *45*, 1882−1897.

(34) Mittal, K. L. *Polyimides and Other High Temperature Polymers: Synthesis, Characterization and Applications*; BSP BV: Netherlands, 2003.

(35) Schwartz, C. J.; Bahadur, S. *Wear* **2000**, *237*, 261−73.

(36) Rapoport, L.; Nepomnyashchy, O.; Lapsker, I.; Verdyan, A.; Moshkovich, A.; Feldman, Y.; Tenne, R. *Wear* **2005**, *259*, 703−707.

(37) Chen, H.; Jacobs, O.; Wu, W.; Rüdiger, G.; Schädel, B. *Polym. Test.* **2007**, *26*, 351−360.

(38) Goyal, R. K.; Tiwari, A. N.; Negi, Y. S. *Mater. Sci. Eng., A* **2008**, *486*, 602−610.

(39) Bahadur, S.; Gong, D. *Wear* **1992**, *154*, 151−165.

(40) Wang, Q. H.; Xue, Q.; Liu, H.; Shen, W.; Xu, J. *Wear* **1996**, *198*, 216−219.